Structures 34 (2021) 158–168

Contents lists available at ScienceDirect

Structures

journal homepage: www.elsevier.com/locate/structures

Effect of building importance factor on seismic performance of rc frame type shopping malls subjected to pulse-like records

Ahmet Güllü [a,*], Genco Karameşe [b]

[a] Department of Civil Engineering, Istanbul Gedik University, Kartal, Istanbul 34876, Turkey
[b] Istanbul Project Coordination Unit, Üsküdar 34692, Turkey

ARTICLE INFO

Keywords:
Building importance factor
Performance evaluation
Response history analyses
Push-over analyses
Seismicity
Performance-based design

ABSTRACT

Since they offer many alternatives for shopping, eating, resting, etc. many people spend a considerable time in shopping mall buildings. Therefore, this type of building is increasing rapidly. The increment rate was almost three in Turkey for the last decade. The recently released seismic code of the country has some serious alterations such as increased seismicity of some regions and reduced performance level limits of structural members. Besides, the building importance factor (I) of the shopping malls was defined clearly to be 1.2 whereas some shopping malls were designed considering $I = 1.0$ and constructed before 2018. Therefore, seismic performances of the shopping malls became questionable according to the code. In this study, seismic performances of two existing shopping mall buildings, which were designed and constructed by considering $I = 1.0$, are investigated based on the recently released seismic code and nonlinear analyses in which the utilized records were scaled considering $I = 1.2$. The results showed that the increased seismicity and reduced performance level limits may lead to excessive story drifts and plastic rotations for some records. However, the mean value of the analysis results satisfies the *life safety (LS)* performance level. Therefore, the importance factor might be suggested to be 1.0 for shopping malls close to the faults to avoid an unnecessary increment of the initial cost.

1. Introduction

Seismic codes of the countries are regularly updated based on the recent achievements in structural and earthquake engineering. Significant alterations in the codes make the seismic performance of some structures doubtful. Therefore, performance-based assessments gained noteworthy popularity in the last decades.

Starting with SEAOC [1], performance-based methods have been developed and implemented in many seismic codes [2–4] for seismic assessment of structures based on nonlinear static procedures or response history analyses. The fast development of the computation techniques in the area also accelerated the application of the method, although computational costs were increased seriously [5]. Krawinkler and Seneviratna [6] investigated the advantages and disadvantages of push-over analysis for seismic performance evaluation. Aydınoğlu [7] proposed an incremental response spectrum analysis based on inelastic spectral displacements for multi-mode performance evaluations. Sürmeli and Yüksel [8] introduced a novel adaptive push-over procedure for *3D* structures subjected to bidirectional shaking. Owing to the developed methods and the technology, the seismic performances of the structures can be evaluated easily. Consequently, many studies focused on the performance evaluation of the distinct type of structures, [9–17]. Yun et al. [9] proposed a performance evaluation technique for steel moment frames based on nonlinear dynamic and reliability theory. Usami et al. [10] investigated the performance of steel arch bridges exposed to major earthquakes through dynamic analyses. Lee [11] compared the seismic performance of diagrid and tubular structures through nonlinear response history analyses (*NRHA*). Khorami et al. [12] investigated the seismic performance of buckling restrained braced frames with varying story numbers. Aslan et al. [13] evaluated the seismic performance of in-plane irregular frame buildings based on *TSC* 2007 [14]. Abraik [15] assessed seismic performance of reinforced concrete (*RC*) moment resisting frames (*MRF*) with hybrid shape memory alloy joints under sequential seismic hazard. Rizwan et al. [16] evaluated the seismic performance of *RC MRF* with low-strength concrete based on *NRHA*. Khan et al. 2021 [17] investigated the seismic performance of *RC MRF* structure built-in crumb rubber by performing shake table tests.

The seismic design of structures is mainly based on two parameters namely global ductility factor and building importance factor. There are

* Corresponding author.
E-mail addresses: ahmet.gullu@gedik.edu.tr (A. Güllü), gkaramese@ipkb.gov.tr (G. Karameşe).

https://doi.org/10.1016/j.istruc.2021.07.075
Received 25 March 2021; Received in revised form 23 July 2021; Accepted 26 July 2021
Available online 4 August 2021

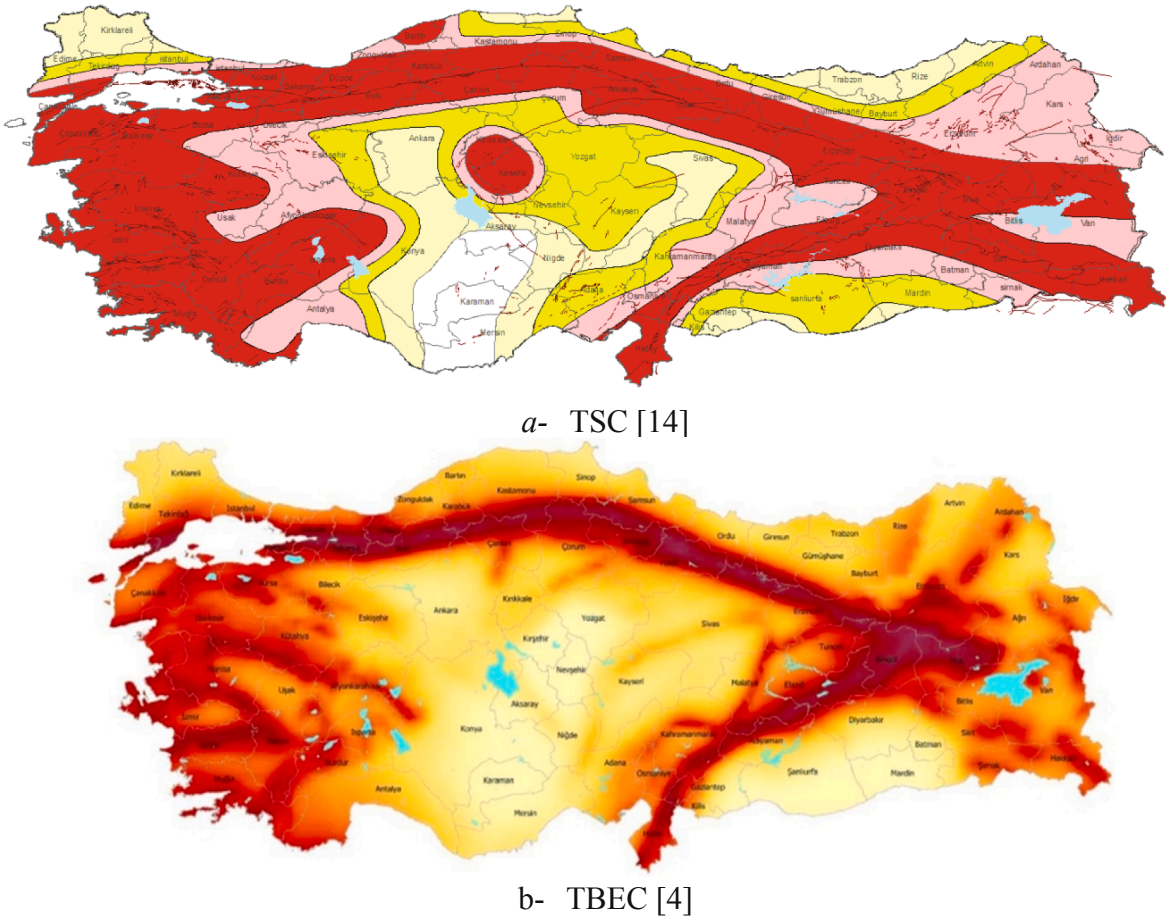

Fig. 1. Seismic hazard maps of Turkey [26].

several studies for the effect of global ductility factor on the seismic performance of the structures, [19–21], while the number is limited for the effect of the importance factor, [18]. The building importance factor, provided by the seismic codes, is a multiplier that increases the design loads of structures based on the occupancy type. The factor mainly aims to sustain the functionality of specific structures after earthquakes. Dhir et al. [18] evaluated the effect of the importance factor on the level of safety and the cost by analyzing 2D frames with distinct story numbers. It was concluded that the damage might be reduced up to 30% by increasing the importance factor from 1.0 to 1.5 while the building cost increases significantly. Jimenez and Morillas [22] investigated the effect of the importance factor on the seismic performance of hospitals constructed in medium seismicity regions. Performance of 2D frames having distinct importance factors was evaluated through FEMA P-58-1 methodology, [23]. The study resulted that the seismic performance of the frames was not sufficient in terms of damage, loss of functionality, and repair cost. Garcia-Perez [24] mentioned that maximum values of ground acceleration for the earthquakes with higher magnitude saturate at near-fault sites. Therefore, smaller importance factors were proposed for that sites. In the study, analyzes were performed to reduce the costs considering Poisson and non-Poisson interarrival time for earthquake occurrence. The study showed that the building importance factor should be smaller for the sites close to the faults.

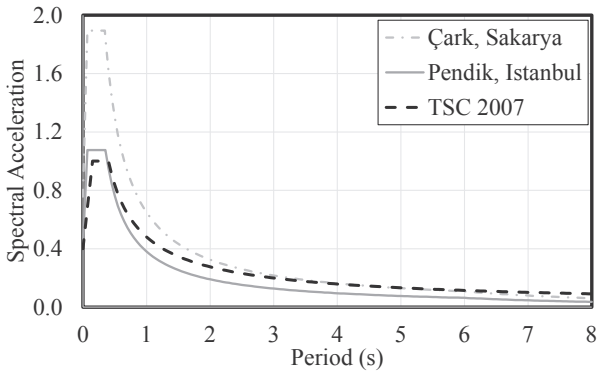

Fig. 2. Design acceleration spectra provided by the seismic codes for Pendik and Çark.

The safety level reached through the increased importance factor might be a good indicator for initial cost and damage cost estimations which is essential for the stakeholders, [18]. Even though the seismic codes dictate the building importance factor, which was decided intuitively, its effect on the seismic performance and the cost of the structure is not investigated for reinforced concrete moment resisting frames, yet. Hence, the rationale of the study is the seismic performance assessment of two shopping mall buildings considering building importance factor, pulse-like records, two locations with different seismicity, and *TBEC* [4]. Nonlinear static and response history analyses (total 88 analyses) were performed on three-dimensional buildings rather than 2D frames. The results are presented in the form of rotation of structural members, inter-story drifts, and base shear.

2. Alterations in TBEC that may affect the seismic performance of structures

The upgraded seismic code of Turkey [4] brought significant alterations for designing the structures. The importance factor (I) of buildings

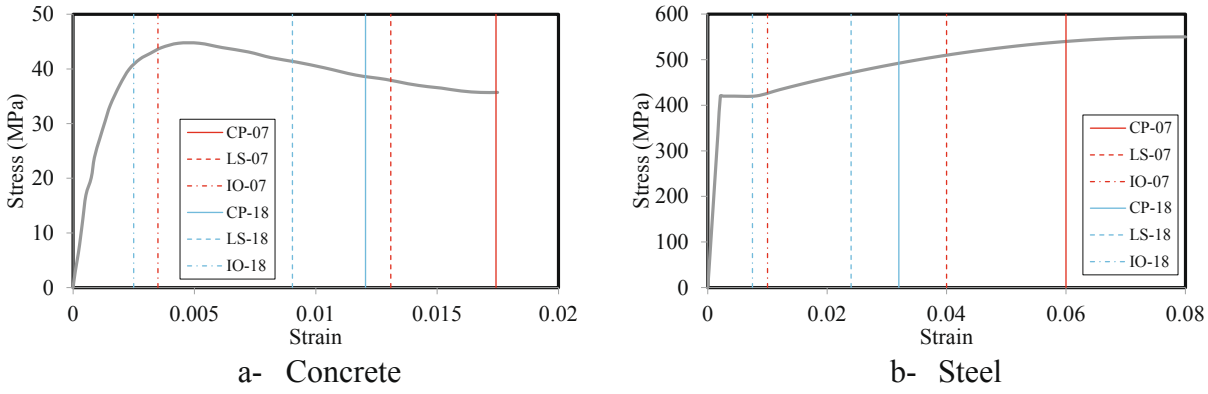

Fig. 3. Calculated performance levels based on the previous and upgraded seismic codes.

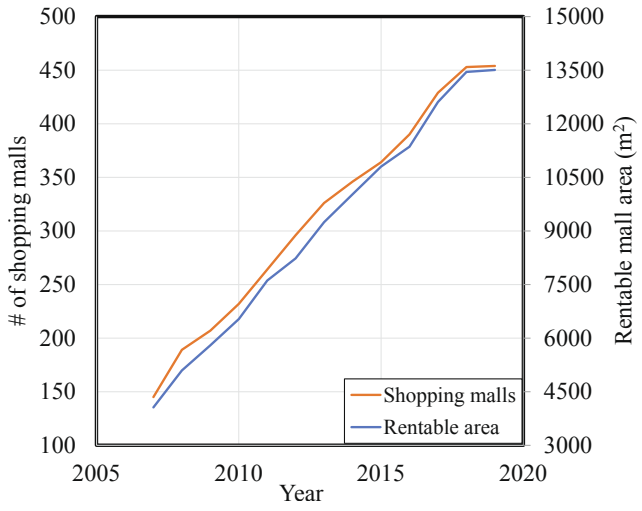

Fig. 4. Increment of total shopping malls and rentable areas in Turkey between 2007 and 2019.

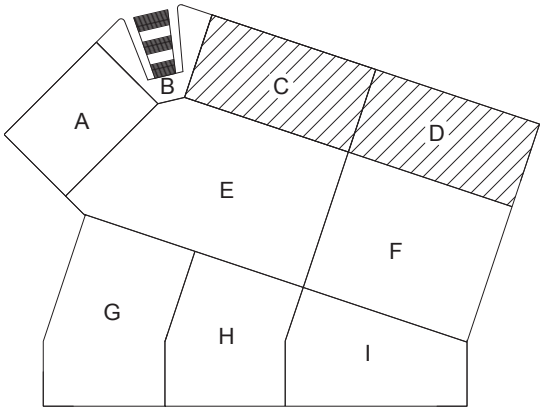

Fig. 5. Plan view of the whole shopping mall and location of the evaluated buildings.

in which many people exist for a short time is suggested to be 1.2 in the previous code, also [14]. However, practitioners designed and constructed some shopping malls by considering $I = 1.0$ since shopping malls were not listed in that type of buildings. The factor was given clearly to be 1.2 for such buildings in the updated code. Hence, there is a discrepancy between some of the constructed buildings and the requirement of *TBEC* [4].

The seismicity of the regions along the main faults was considerably increased, also. The previous seismic risk map consisted of only five earthquake zones, Fig. 1a. In this map, the same spectral acceleration spectrum was proposed for the design of buildings in the regions around the faults. However, the upgraded map is a product of an extensive micro-zonation study [25], Fig. 1b.

As an illustrative example, design acceleration spectra of the Pendik district of Istanbul and Çark district of Sakarya, which are located around the North Anatolian Fault, are compared in Fig. 2. Same spectra (black dashed line) were defined for these regions in *TSC* [14]. Although the proposed spectra by the former [14] and updated codes [4] are comparable for Pendik (gray solid line), there is a significant difference for Çark (gray dotted dashed line), especially around the plateau region.

In addition to increased seismicity, performance levels of construction materials were reduced significantly by *TBEC* [4], see Fig. 3. In the figure, *CP*, *LS,* and *IO* correspond to collapse prevention, life safety, and immediate occupancy performance levels, respectively. The numbers written next to the abbreviations are identified as the releasing year of the seismic codes. The resultant performance levels of the upgraded code are considerably lower than the limits of the previous code. For both of the materials (confined concrete and steel), the *LS* performance limit of *TSC* [14] is greater than the collapse limit of *TBEC* [4].

3. Shopping malls in Turkey

Owing to some social advantages, shopping malls have gained high popularity in Turkey especially after the first years of the 2010s. There were a total of 145 shopping malls in 2007 whereas the number has reached 454 in 2019, Fig. 4. The rentable area was also increased to 13508 m^2 from 4063 m^2 in the same period. Increments in both the number of shopping malls and rentable areas were almost linear until 2018 and practically parallel to each other.

Most of the shopping malls (147 of 454) were constructed in Istanbul where there were only 25 shopping malls in 2004 [27]. The rapid increase of the shopping malls around the city shows that they are an important part of daily social life. People prefer visiting the shopping malls for mostly socialization (sports centers, cafes, game studios, etc.) and finding their all needs in one space, [27]. The high interest has also affected the underground system of the city. Most of the stations have direct connections to the shopping malls.

Since they are highly preferred by the citizens even during the covid-19 pandemic, an investigation for the earthquake performance of such buildings considering *TBEC* [4] is essential.

4. Case study

Two shopping mall buildings constructed by assuming $I = 1.0$ are numerically evaluated considering *TBEC* [4] in this study, [28]. The

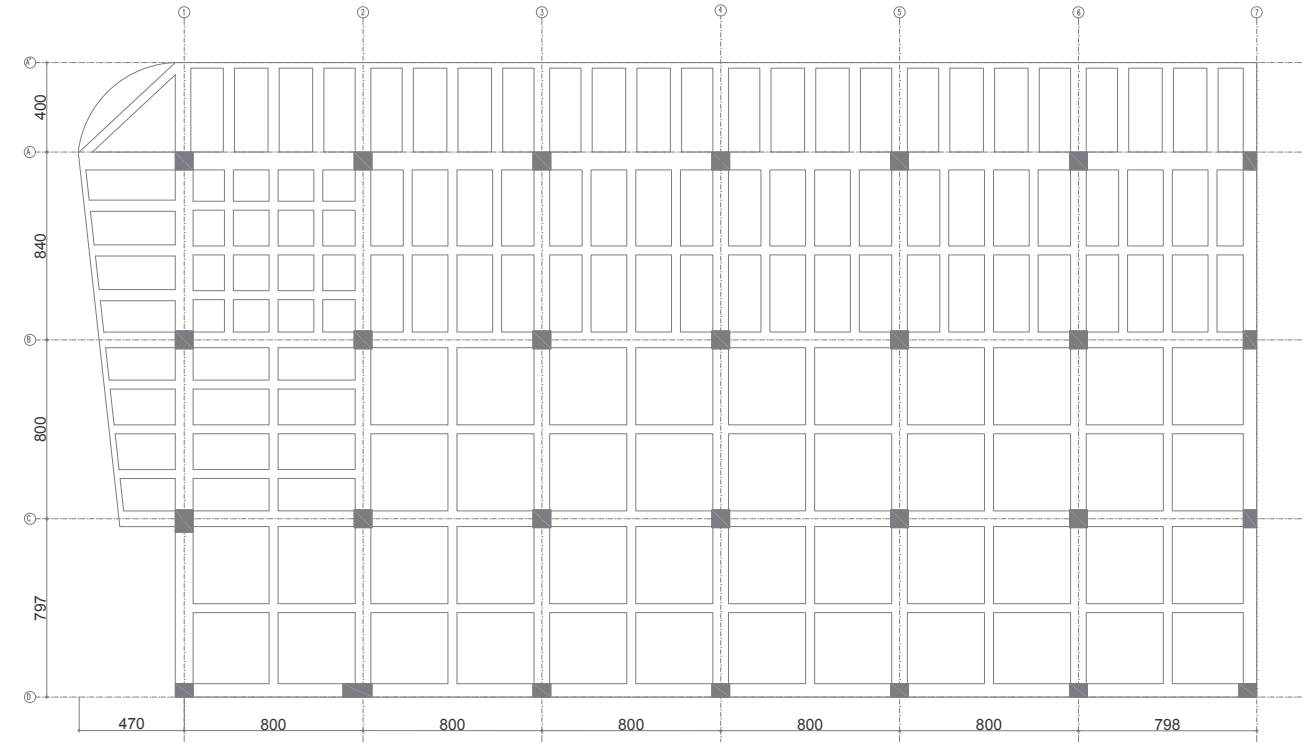

a- Building C

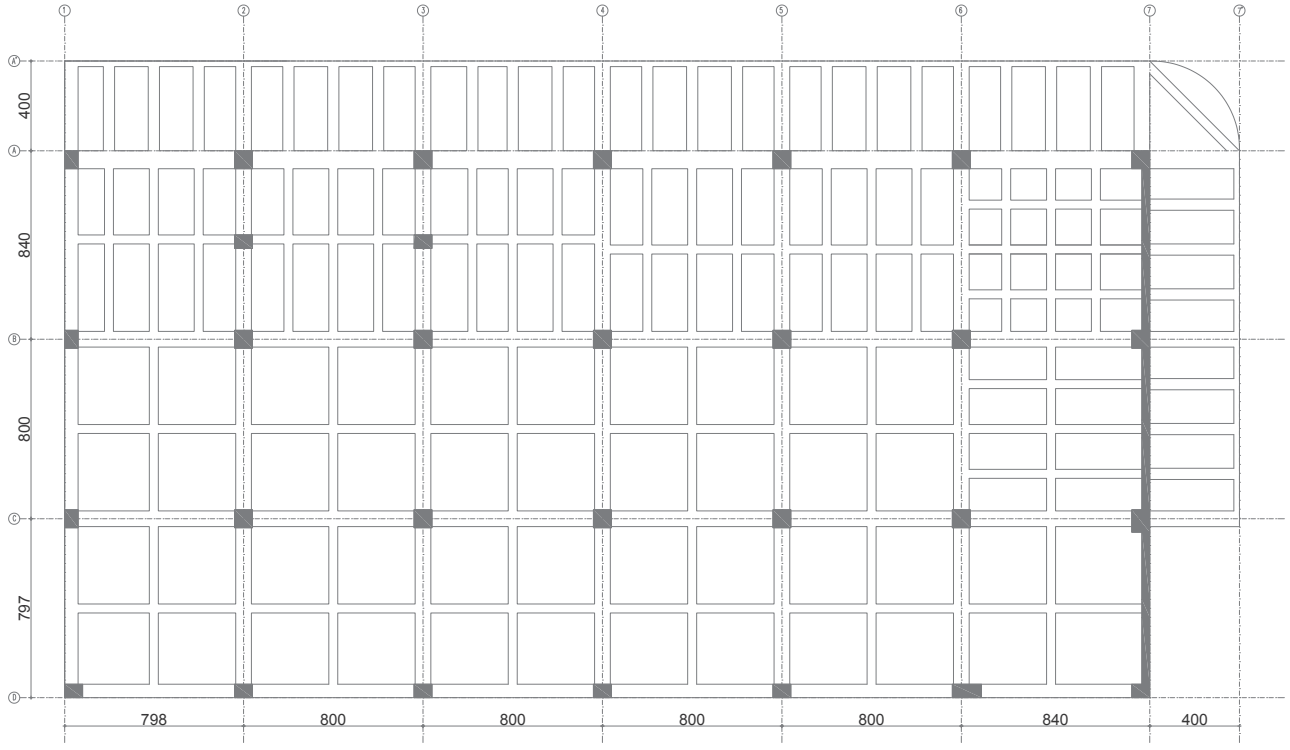

b- Building D

Fig. 6. General plan views of the evaluated buildings (dimensions are in cm).

utilized records were scaled by considering $I = 1.2$ to investigate the effect of the factor. The shopping malls should satisfy *LS* performance level for *DD-2* ground motion level which corresponds to 10% exceedance in 50 years with a return period of 475 years. The code requires nonlinear analyses for the performance evaluation.

4.1. Description of the buildings

Originally, the buildings (*Buildings C* and *D*) studied in this paper were constructed in Pendik, Istanbul. The placement of the evaluated buildings (hatched areas) in the whole complex is shown in Fig. 5.

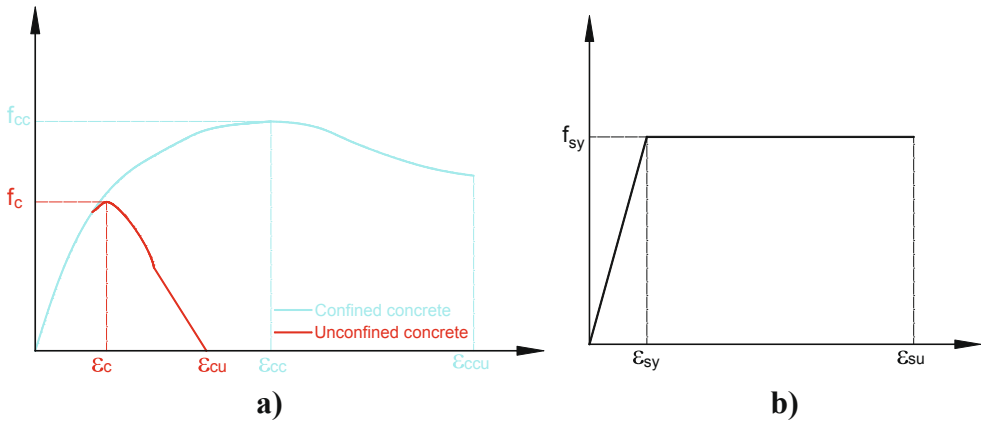

Fig. 7. Employed material models for **a)** concrete and **b)** rebar.

Table 1
Numerical model parameters for concrete and rebars.

Concrete	Elasticity Modulus (GPa)	Comp. strength f_{ck} (MPa)	Tensile str. f_{ctk} (MPa)	Self-weight γ_c (kN/m^3)
	33	35	2.1	25.0
Rebar	Elasticity Modulus (GPa)	Yielding str. f_{yk} (MPa)	Ultimate strain ε_{su} (%)	Self-weight γ_s (kN/m^3)
	200	420	9	78.5

The buildings have almost rectangular floor plans with 28.37 m in depth and, 48.37 m (Building C), and 52.37 m (Building D) in length. There are also plan extensions that reach almost 4.7 m around the buildings. The buildings have three stories with 6.0 m in height. Both of them have seven and four *RC* frames on the longitudinal (frames 1–7) and transversal (frames A-D) directions, respectively. All longitudinal and transversal frames were spaced almost 8.0 m. Plan views of the buildings are depicted in Fig. 6a and b.

Slab thicknesses are uniform and 17 cm for both buildings. Primary and secondary beams have 700×700 mm^2 and 400×700 mm^2 cross-sections, respectively. Similarly, cantilever and edge beams have 700 mm height while their width is 500 and 250 mm, respectively. Primary beams which support the cantilevers have a width of 800 mm. In general, square and rectangular columns have 800×800 mm^2 and 600×800 mm^2 cross-sections, respectively. Only, the column on the conjunction of *1* and *C axes* of *Building C* has an 800×1000 mm^2 cross-section, as well as the column on the conjunction of *6* and *D* axes of *Building D* has a 600×1300 mm^2 cross-section. *Building D* has also a retaining wall in the first story of the rightmost frame with a thickness of 350 mm. Details of typical reinforcement of structural members are given as supplementary data.

For the construction of the buildings, concrete having a compressive strength of 35 MPa as well as rebars with 420 MPa yielding strength were preferred.

4.2. Numerical modeling

Three-dimensional (*3D*) numerical models of the buildings were generated using frame elements for beams and columns by ETABS software, [28]. The columns were fixed at the base level. Seismic mass was calculated considering the assigned dead and live loads with coefficients of 1.0 and 0.6, respectively [4]. The considered dead loads were self-weight of the structural members (25 kN/m^3) and 3.5 kN/m^2 for claddings. Additionally, a 5.0 kN/m^2 live load was assigned. The dead and live loads assigned to the roof floor were 4.0 kN/m^2 and 2.0 kN/m^2, respectively.

Geometric and material nonlinearities were considered in the models. The material behavior of the concrete and the rebars were represented by using well-known Mander [29] and bilinear models, Fig. 7a and b. In Fig. 7a, f_{cc} and f_c are compressive strengths of confined and unconfined concrete, respectively. Additionally, strains at maximum strength and ultimate case are shown with ε_c and ε_{cu} for unconfined concrete as well as ε_{cc} and ε_{ccu} for confined concrete. In Fig. 7b, yield strength, yield strain, and ultimate strain of the rebar are shown by f_{sy}, ε_{sy}, and ε_{su}, respectively. The input parameters of the materials are given in Table 1.

The nonlinear behavior of the structural members was simulated through lumped plasticity. Plastic hinge length was adopted as half of the bending depth considering the suggestions of *TBEC* [4].

Table 2
Obtained natural periods of the evaluated buildings.

Direction	Building C	Building D
Longitudinal	1.015 s	1.132 s
Transversal	1.068 s	1.119 s

5. Analyses results and performance evaluation

The vulnerability of the considered buildings is assessed by considering some engineering demand parameters (*EDPs*) obtained from *NRHA* e.g. story drifts, base shears, and rotations of structural members. When the limit values defined in [4] are exceeded, the buildings are considered vulnerable.

At first, modal analyses were performed and vibrational modes in each direction of each building were obtained as shown in Table 2.

TBEC [4] imposes nonlinear analyses (static and/or dynamic

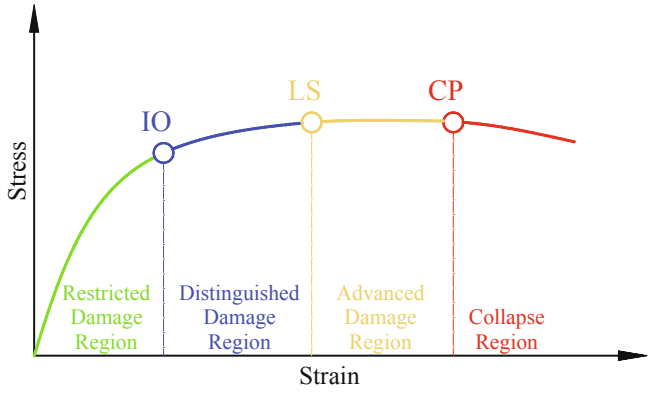

Fig. 8. Performance levels and damage regions defined in *TBEC* [4].

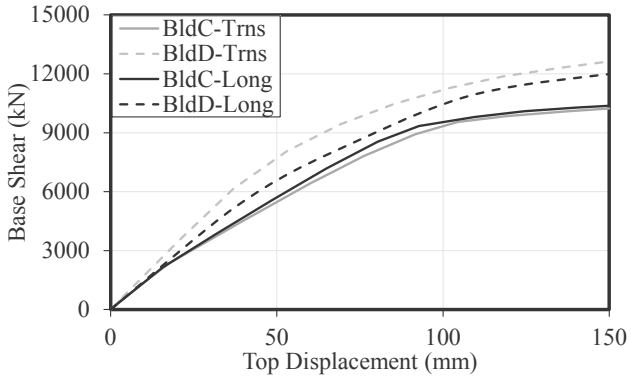

Fig. 9. Push-over curves of the buildings.

response history) for the performance evaluation. In this study, a single-mode push-over method was employed, since the buildings satisfy the following conditions;

- The torsional irregularity coefficient of each story calculated without considering any eccentricity must be smaller than 1.4.
- Participated mass ratio of the first mode must be higher than 70%.

According to the code, the buildings should satisfy the *LS* performance level for the *DD-2* earthquake. Besides, the following conditions must be satisfied.

- Up to 35% of the beams of any story may experience advanced damage (see Fig. 8) as a result of performed nonlinear analyses in each direction.
- The ratio of the shear force experienced by the vertical elements with advance damage to the total story shear must be below 20%. The ratio might be increased to 40% for the top floor.
- All the other structural elements should be in *restricted* or *distinguished* damage regions. However, the ratio of the shear forces carried by the vertical elements that have been exceeded by both upper and lower sections on any floor should not exceed 30% of the shear force carried by all the vertical elements on that floor.

The plastic rotation (θ_p) of a plastic hinge should be lower than the value calculated by Eq. (1) to satisfy the *CP* performance level, [4]. In the equation, ϕ_u and ϕ_y are ultimate and yield curvature, L_p is plastic hinge length, $L_s$is shear span, andd_b is the average diameter of the longitudinal rebars. The limit value for the plastic rotation to satisfy the *LS* performance level is 75% of θ_p^{CP}, Eq. (2). No plastic rotation is allowed for *IO* performance, [4], Eq. (3).

$$\theta_p^{CP} = \frac{2}{3}\left[(\phi_u - \phi_y)L_p\left(1 - 0.5\frac{L_p}{L_s}\right) + 4.5\,\phi_u\,d_b\right] \quad (1)$$

$$\theta_p^{LS} = 0.75\,\theta_p^{CP} \quad (2)$$

$$\theta_p^{IO} = 0 \quad (3)$$

5.1. Nonlinear static analyses

Each story of the buildings was exposed to statically incremental lateral loads which are proportional to the first mode shape of the undamaged structure. The obtained push-over curves for buildings in both directions are depicted in Fig. 9. In the figure, solid and dashed lines stand for *Building C* and *Building D*, respectively. Additionally, the longitudinal direction is represented by black lines whereas gray lines denote transversal direction. The buildings have almost similar behavior in both directions.

Table 3
Displacement demands of the buildings which calculated by the nonlinear static procedure.

Building	Location	S_{ae} (g)		S_{di} (m)		u_{top} (m)	
		Long	Trns	Long	Trns	Long	Trns
C	Pendik, İstanbul	0.375	0.357	0.096	0.101	0.132	0.139
	Çark, Sakarya	0.639	0.608	0.164	0.172	0.225	0.236
D	Pendik, İstanbul	0.337	0.341	0.107	0.106	0.146	0.249
	Çark, Sakarya	0.573	0.580	0.183	0.181	0.144	0.245

Using push-over and capacity curves modal top displacement demands of the buildings were calculated, [4]. The obtained modal displacements (d) converted to the physical displacement (u_{1n}) by Eq. (4) where ϕ_1 and $\Gamma_1$are modal displacement vector and modal participation factor of the first vibrational mode.

$$d_1 = \frac{u_{1n}}{\phi_1\,\Gamma_1} \quad (4)$$

The resultant pseudo-spectral acceleration (S_{ae}), spectral displacement (S_{di}), and top displacement demands (u_{top}) of the buildings are tabulated in Table 3. In the table, longitudinal and transversal directions were abbreviated as *Long* and *Trns*, respectively.

Rotations of the beams and columns of the evaluated buildings are classified considering the Eqs. (1-3). Most of the structural members satisfied life safety performance level. A few beams (13.5%) of the first story reached to collapse prevention performance level in the case of Çark, Sakarya.

5.2. Nonlinear response history analyses

The buildings were exposed to bi-directional pulse-like ground motions since they are located quite close to the *North Anatolian Fault*. The effect of vertical ground motions is neglected because the conditions of the code [4] were satisfied.

5.2.1. Selection and scaling of ground motion records

TBEC [4] requires at least eleven ground motion records for the performance evaluations of building-type structures. Further, selected records should be compatible with the seismic characteristics of the region such as distance to fault, faulting mechanism, and local soil profiles. Each horizontal record should be applied to each horizontal direction of the buildings. Hence one building requires twenty-two *NRHA* for the performance analyses.

In case of the existence of any record from the building region, these records must be utilized in the analyses. The number of records sourced from the same earthquake was restricted to three. Since the requirements of the code are so strict, reaching an insufficient number of records is highly possible.

Selected records should be scaled considering the amplitude of spectral accelerations between 0.2 T_1 and 1.5 T_1 where T_1 is the first vibrational period of the structure. The amplitudes of the scaled records should not be lower than the design acceleration spectrum in this range. In the case of *3D* analyses, the horizontal records should be combined by the *SRSS* rule and the design acceleration spectrum should be increased by 30%. A single scaling factor was allowed to employ for both of the horizontal records.

Considering the above-mentioned requirements of the code; ground motion records given by Table 4 are selected for the numerical analyses, [30]. Since North Anatolian Fault has a strike-slip mechanism [31], all the records have this property also. Even though there are not specific values, the average shear velocity of the upper 30 m soil deposits (V_{s30}) of the considered sites can be assumed between 400 and 1200 m/s,

Table 4
Some characteristics of the selected records.

#	RSN	Earthquake Name	Magnitude	R_{rup} (km)	V_{s30} (m/s)	T_p (s)	PGV (cm/s)	PI
1	150	Coyote Lake	5.74	3.11	663.31	1.232	44.3	1.000
2	451	Morgan Hill	6.19	0.53	561.43	1.071	78.4	1.000
3	459	Morgan Hill	6.19	9.87	663.31	1.232	36.5	1.000
4	568	San Salvador	5.80	6.30	489.34	0.805	79.9	1.000
5	569	San Salvador	5.80	6.99	455.93	1.127	72.9	1.000
6	1161	Kocaeli_Turkey	7.51	10.92	792.00	5.992	44.6	1.000
7	1165	Kocaeli_Turkey	7.51	7.21	811.00	5.369	38.3	1.000
8	2734	Chi-Chi_Taiwan-04	6.20	6.20	553.43	2.436	43.5	1.000
9	4040	Bam_Iran	6.60	1.70	487.40	2.023	124.1	1.000
10	4103	Parkfield-02_CA	6.00	4.23	410.40	0.700	32.3	0.999
11	8164	Duzce_Turkey	7.14	2.65	690.00	10.052	38.9	1.000

Table 5
Calculated scale factors.

#	RSN	Earthquake Name	Pendik, Istanbul	Çark, Sakarya
1	150	Coyote Lake	1.6257	2.8616
2	451	Morgan Hill	0.5142	0.9051
3	459	Morgan Hill	1.8675	3.0905
4	568	San Salvador	0.8940	1.5736
5	569	San Salvador	1.2382	2.1795
6	1161	Kocaeli_Turkey	2.3230	4.0890
7	1165	Kocaeli_Turkey	2.4884	4.3801
8	2734	Chi-Chi_Taiwan-04	1.1449	2.0152
9	4040	Bam_Iran	0.7819	1.3325
10	4103	Parkfield-02_CA	1.3608	2.3200
11	8164	Duzce_Turkey	1.4656	2.5002

[32–33]. Hence, the selected records have V_{s30} values in this range. In the table, *RSN* is the record sequence number, R_{rup} is the distance to rupture, T_p is the pulse period, and *PI* is the pulse indicator calculated through the relations are given by Panella et al. [34]. In the study, the pulse index of a record was defined based on velocity time history and peak ground velocity (*PGV*) of the record. The record was considered as pulse-like if its pulse index exceeds 0.7 and *PGV* is greater than 30 cm/s.

The scaling procedure consists of two steps. The first step minimizes the difference between the target, which is constructed by considering a building importance factor of 1.2, and the response spectra. 5% damped acceleration response spectra of the selected records are calculated by a piece-wise algorithm, [35–36], and compared with the target. Hereafter, ratios of the target to the response spectra are calculated in the prescribed period range (0.2–1.5 T_1). Finally, the first scaling factor is calculated to be the mean value of the ratios. Since the code does not allow a lower amplitude in the considered scaling range of response spectra, the maximum difference between the target and the initially scaled response spectra was calculated in the second step. The final scale factor was determined by the multiplication of the calculated scaling factors, [37]. The scaling procedure does not affect the frequency content of the record.

The scaling factors calculated for the regions are given in Table 5. The strict rules for selecting and scaling ground motion records resulted in relatively higher scale factors for some records. Acceleration response spectra of the scaled records and their mean are given in Fig. 10.

5.2.2. Plastic rotations of beams and columns

TBEC [4] requires performance evaluation based on plastic rotations of the structural members. Limits for the element rotations are calculated by Eqs. (1-3). Average values of the rotations resultant from 22 *NRHA* for each building and region are compared with the predefined limits.

The analyses resulted in some collapsed beams and columns with advance damage for some specific records in both locations. However, average plastic rotations of all beams and columns were found to be in

Table 6
Maximum plastic rotations of the structural members.

Element Type	C, Çark	C, Pendik	D, Çark	D, Pendik
	rad	rad	Rad	rad
Beam	0.0342	0.0110	0.0096	0.0062
Column	0.0050	0.0023	0.0055	0.0024

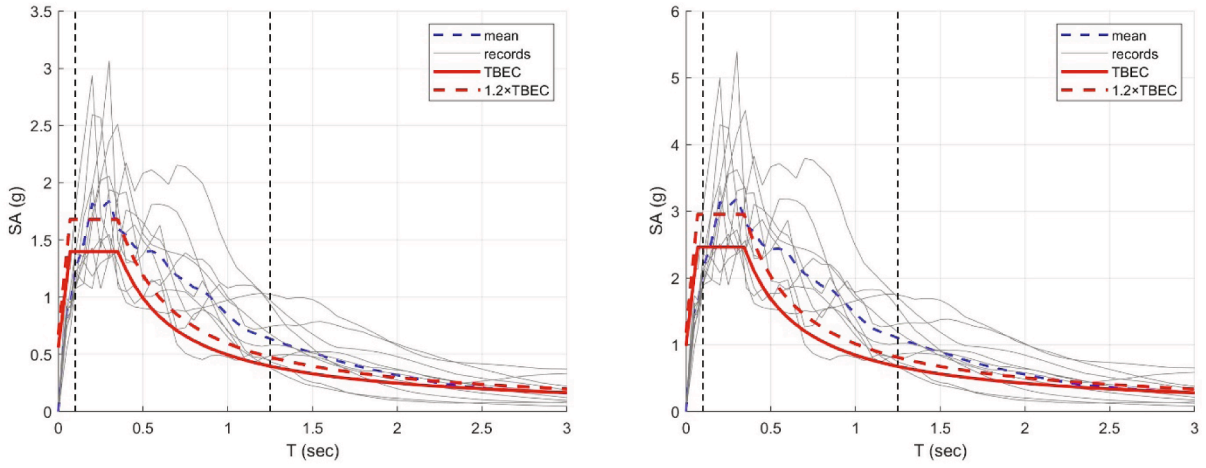

Fig. 10. Spectral accelerations of scaled records and target spectrum.

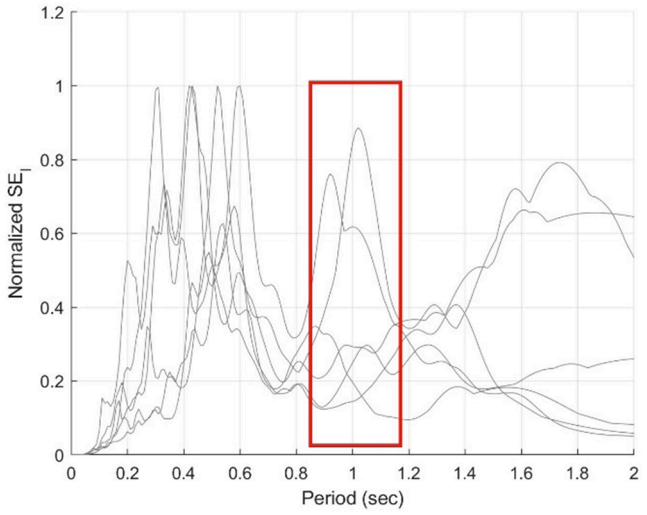

Fig. 11. Normalized seismic energy spectra of Kocaeli and Düzce records.

distinguished damage zone. The absolute maximum rotations were recorded generally at the edge and corner columns of the first story. Additionally, maximum rotations were obtained on the main beams having mostly 70×50 cm^2 and 70×70 cm^2 cross-sections. The obtained maximum rotations for the structural members are tabulated in Table 6.

Although the average rotations obtained for structural members mainly correspond to the *LS* performance level, the buildings reached to *CP* performance level for Kocaeli and Düzce records. To investigate the possible reasons, the energy balance concept is preferred, since the seismic input energy and hysteretic energy are promising indicators of the damage, [38–40], Eq. (5). In the equation, M, C, and F(u) are mass, damping, and restoring force characteristics of a single-degree of freedom system. Additionally, u is the relative displacement and dots represent its derivatives, as well as subscript g, denotes ground level. The terms of the equation are known as kinetic energy, damping energy, strain energy, and total input energy (SE_I), respectively. Strain energy has also two sub-components namely elastic strain energy and hysteretic energy. Using Eq. (5) and the piece-wise algorithm (33–34), the elastic 5% damped seismic input energy spectra of the records are plotted in Fig. 11. Since each record has a distinct energy response, the spectra are normalized by their maximum values. As highlighted in the figure, the records have a dominant region around the period range of analyzed buildings. This may lead to excessive deformations in structural members.

$$M\int \ddot{u}\dot{u}dt + C\int \dot{u}^2 dt + \int F(u)\dot{u}dt = -M\int \ddot{u}_g \dot{u}dt \tag{5}$$

5.2.3. Inter-story drift ratios

The allowable drift ratio is given by Eq. (6) in *TBEC* [4]. In the equation, $\delta_i$and h_i are maximum horizontal displacement and height of the i^{th} story, respectively. λ is the ratio of spectral acceleration at the first vibration period of the building for *DD-3* level earthquake (50% exceedance in 50 years with a return period of 72 years) to that of *DD-2* level earthquake. Finally, κ is a scaler value which is 1 for *RC* structures and 0.5 for steel structures. In the case of having a flexible infill masonry wall and façade element connection, the constant terms of the equation can be increased to 0.016.

$$\lambda\frac{\delta_i}{h_i} \leqslant 0.008\kappa \tag{6}$$

The spectral accelerations and resultant drift limits are given in Table 7. It is found that the allowable drift limits are almost 2.0% and 2.3% for the buildings in Pendik and Çark, respectively.

In many cases, the drift limit is not exceeded. However, similar to plastic rotations of structural elements, the maximum story drifts reached up to 6% for Kocaeli and Düzce records. As it was shown in the previous section, the frequency content of these records overlaps with the buildings' dominant frequencies.

5.2.4. Base shear

The resultant base shears (V_{base}) of 88 *NRHA* are normalized with the weight (*W*) of the buildings. The obtained unitless coefficients (medians, standard deviations, etc.) are illustrated in Fig. 14. In the figure solid (for

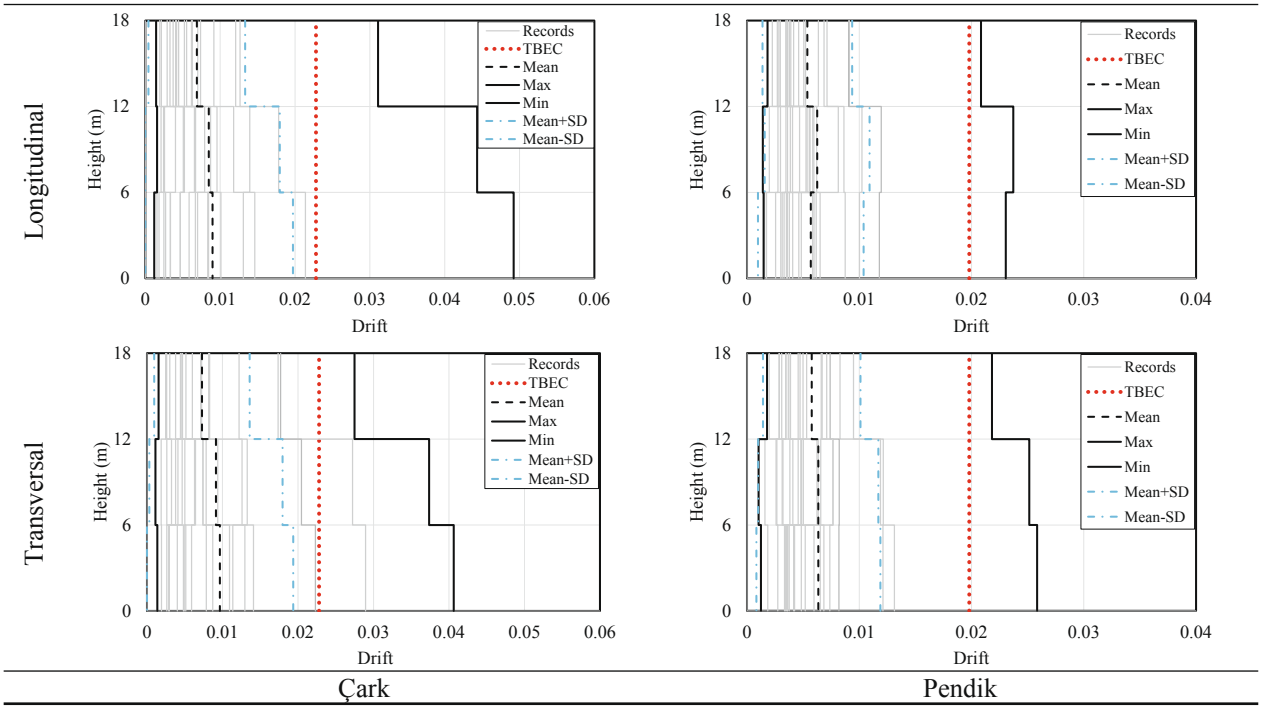

Fig. 12. Inter-story drift ratios of Building C for different locations.

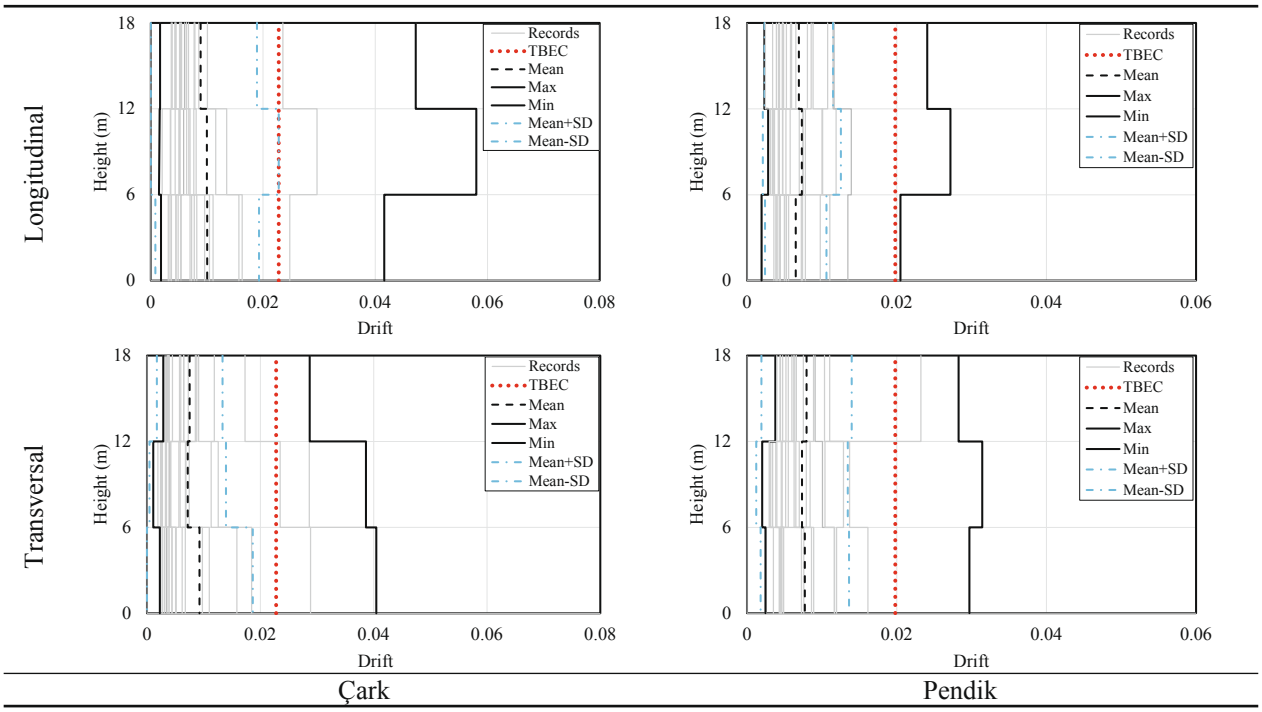

Fig. 13. Inter-story drift ratios of Building D for different locations.

Table 7
Determination of allowable drift levels.

Building	Direction	Pendik, Istanbul				Çark, Sakarya			
		$SA_{DD\text{-}2}$ (g)	$SA_{DD\text{-}3}$ (g)	λ	Drift (%)	$SA_{DD\text{-}2}$ (g)	$SA_{DD\text{-}3}$ (g)	λ	Drift (%)
C	Long.	0.381	0.154	0.404	1.98	0.649	0.228	0.351	2.28
	Trans.	0.363	0.147	0.405	1.98	0.619	0.217	0.351	2.28
D	Long.	0.331	0.134	0.404	1.98	0.565	0.198	0.350	2.28
	Trans.	0.331	0.134	0.405	1.98	0.565	0.198	0.350	2.28

The resultant inter-story drift ratios are given in Figs. 12 and 13 for buildings *C* and *D*, respectively.

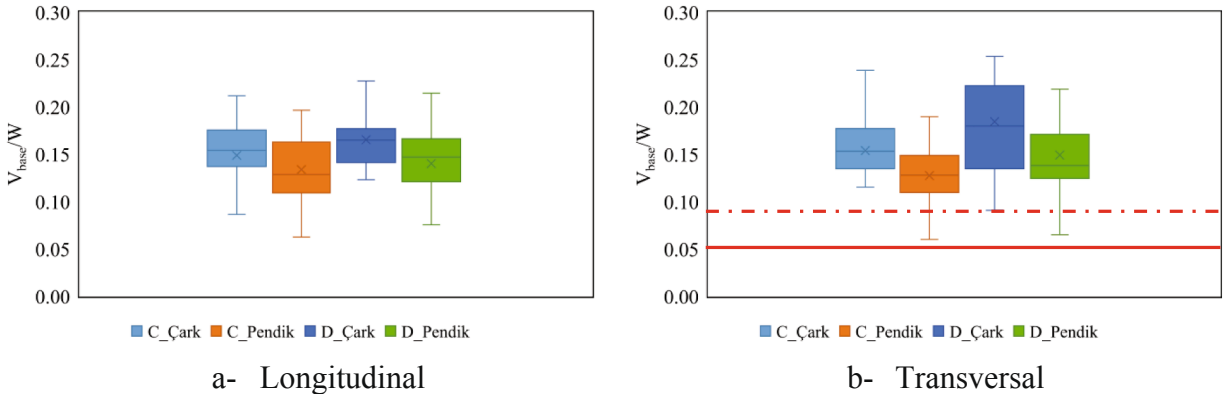

Fig. 14. Obtained base shear coefficients.

Pendik) and dashed (for Çark) red lines correspond to minimum base shear coefficients allowed by the upgraded code, [4], which can be calculated by Eq. (7). In the equation, *I* and S_{DS} stand for building importance factor and spectral acceleration at plateau region, respectively.

$$\frac{V_{base}}{W} \geqslant 0.04\ I\ S_{DS} \tag{7}$$

Unitless base shear ratios reached 0.25 and 0.30 for longitudinal and transversal direction where the minimum values are determined to be 0.05 for Pendik and 0.09 for Çark. The analyses showed that all the mean values are above the minimum requirement of the code. However, lower base shear than the limit given by *TBEC* [4] was obtained for a few records.

6. Conclusion

In this study, the seismic performance of two shopping mall buildings was evaluated based on the *Turkish Building Seismic Code* [4] and nonlinear analyses to investigate the effect of the building importance factor (*I*). The buildings were originally designed and constructed considering I = 1.0, while it had to be adopted as 1.2, [4]. A total of 88 nonlinear response history analyses were performed to serve this purpose. The records were scaled by considering 1.2 times increased design acceleration spectra of the regions. Based on the analyses, the following conclusions can be drawn.

For the effect of building importance factor;

- Even though the studied buildings were constructed by assuming $I = 1.0$, the mean values of the analyses have satisfied the requirements of the life safety performance level for the records scaled by considering 1.2 times increased design acceleration spectra.
- Some acceleration data, which were recorded from locations near both Istanbul and Sakarya caused collapse prevention performance since their frequency contents overlap with the dominant frequencies of the buildings. For these records, drift ratios reach up to 4–6% which is fairly beyond the allowable limit.
- Since the performance level has been satisfied, the building importance factor of the shopping malls which are close to the faults might be suggested to be 1.0 if the building satisfies the general requirements of the previous code [14], e.g. strong column – weak beam principle. Otherwise, using greater building importance factors will just increase the initial cost.
- Due to the design acceleration spectrum of the Çark, Sakarya region, the selected records have higher scaling factors. As expected, using higher scale factors resulted in more plastic deformations and greater floor level responses. For instance, the maximum drift ratio was obtained to be about 3.0% for Pendik, Istanbul whereas the value reached up 6.0% for Çark, Sakarya.

For the other considered parameters;

- Performance limits for steel and concrete materials are significantly reduced by the updated code, [4]. Generally, the life safety performance limit of the previous seismic code [14] is higher than that provided for the collapse prevention performance of *TBEC* [4].
- The imposed strict rules for the selection of earthquake records may prevent reaching either a necessary number of the records or smaller scaling factors. To overcome this issue, the effect of the restricted parameters (faulting mechanism, distance to rupture, etc.) on the seismic performance of different structures would be studied.

Declaration of Competing Interest

The authors declare that they have no known competing financial interests or personal relationships that could have appeared to influence the work reported in this paper.

Acknowledgment

The building data was provided by Mr. Ersin Yıldız and Mr. Engin Taşçı from Pendik Municipality. The contribution is gratefully acknowledged.

References

[1] Structural Engineers Association of California (SEAOC) Vision 2000 Committeee. Performance based seismic engineering of buildings; 1995.
[2] FEMA P-58. Seismic performance assessment of buildings. Federal Emergency Management Agency 2012.
[3] American Society of Civil Engineers. Seismic evaluation and retrofit of existing buildings. ASCE/SEI 41-13, Reston, VA; 2013.
[4] Turkish Building Earthquake Code. Specifications for buildings to be built in seismic areas. Ministry of Public Works and Housing, Ankara, Turkey; 2018.
[5] Swensen DJ, Kunnath SK. Consequences of modelling choices in seismic performance assessment of buildings. Earthquake Spectra 2018;34(2):423–40.
[6] Krawinkler Helmut, Seneviratna GDPK. Pros and Cons of a push-over analysis of seismic performance evaluation. Eng Struct 1998;20(4-6):452–64.
[7] Aydınoğlu MN. An incremental response spectrum analysis procedure based on inelastic spectral displacements for multi-mode seismic performance evaluation. Bull Earthquake Eng 2003;1:3–36.
[8] Sürmeli M, Yüksel E. An adaptive modal push-over analysis procedure (VMPA-A) for buildings subjected to bi-directional ground motions. Bull Earthquake Eng 2018;16(11):5257–77.
[9] Yun SY, Hamburger RO, Cornell CA, Foutch DA. Seismic performance evaluation for steel moment frames. J Struct. Eng. 2002;128:534–45.
[10] Usami T, Lu Z, Ge H, Kono T. Seismic performance evaluation of steel arch bridges against major earthquakes. part 1: dynamic analysis approach. Earthquake Engng Struct. Dyn. 2004;33:1337–54.
[11] Kim J, Lee YH. Seismic performance evaluation of diagrid system buildings. Struct. Design Tall Spec. Build. 2012;21:736–49.
[12] Khorami M, Khorami M, Alvansazyazdi M, et al. Seismic performance evaluation of buckling restrained braced frames (BRBF) using incremental dynamic analysis method (IDA). Earthquakes and Structures 2017;13(6):531–8.
[13] Arslan Guray, Borekci Muzaffer, Sahin Baris, Denizer M Ilker, Duman Kutay S. Performance evaluation of in-plan irregular RC frame buildings based on Turkish seismic code. Int J Civ Eng 2018;16(3):323–33.
[14] Turkish Seismic Code Specifications for buildings to be built in seismic areas. Ministry of Public Works and Housing, Ankara, Turkey; 2007.
[15] Abraik Emad. Seismic performance of shape memory alloy reinforced concrete moment frames under sequential seismic hazard. Structures 2020;26:311–26.
[16] Rizwan Muhammad, Ahmad Naveed, Naeem Khan Akhtar. Seismic performance assessment of reinforced concrete moment resisting frame with low strength concrete. Structures 2021;30:1140–60. https://doi.org/10.1016/j.istruc.2020.10.038.
[17] Khan Izzat, Shahzada Khan, Bibi Tayyaba, Ahmed Asfandyar, Ullah Hanif. Seismic performance evaluation of crumb rubber concrete frame structure using shake table test. Structures 2021;30:41–9.
[18] Dhir PK, Zade PZ, Basu A, Davis R, Sarkar P. Implications of importance factor on seismic design from 2000 SAC-FEMA perspective. ASCE-ASME J. Risk Uncertainty Eng. Syst., Part A. Civ. Eng. 2020;6(2):04020016.
[19] Su RKL, Tang TO, Lee CL. Evaluation of local and global ductility relationships for seismic assessment of regular masonry-infilled reinforced concrete frames using a coefficient-based method. Earthquakes and Structures 2013;5(1):1–22.
[20] Fakharifar M, Sharbatdar MK, Lin Z, Dalvand A, Sivandi-Pour A, Chen G. Seismic performance and global ductility of RC frames rehabilitated with retrofitted joints by CFRP laminates. Earthquake Engineering and Engineering Vibration 2014;13(1):59–73.
[21] Avilés Javier, Eduardo Pérez-Rocha Luis. Use of global ductility for design of structure–foundation systems. Soil Dyn Earthquake Eng 2011;31(7):1018–26.
[22] Jimenez FJP, Morillas L. Effect of importance factor on the seismic performance of health facilities in medium seismicity regions. J Earthquake Eng 2019. https://doi.org/10.1080/13632469.2019.1691680.
[23] Federal Emergency Management Agency. FEMA P-58-1: Seismic performance assessment of buildings. Volume 1-methodology. 2012, Washington, DC: FEMA.
[24] García-Pérez Jaime, Castellanos Francisco, Díaz Orlando. Occupancy importance factor in earthquake engineering. Eng Struct 2005;27(11):1625–32.
[25] Giardini Domenico, Danciu Laurentiu, Erdik Mustafa, Şeşetyan Karin, Demircioğlu Tümsa Mine B, Akkar Sinan, et al. Seismic hazard map of the Middle East. Bull Earthquake Eng 2018;16(8):3567–70.
[26] AFAD Disaster & Emergency Management Authority, Presidential of Earthquake Department.
[27] Çakır Zeytinoğlu F, Uydacı M, Çağlayan Akay E, et al. İstanbul'daki alışveriş merkezleri üzerine bir araştırma: kümeleme analizi. Social Sciences Research Journal 2016;5(1):111–28. in Turkish.
[28] ETABS v15, CSI America, https://wiki.csiamerica.com/display/etabs/Home.
[29] Mander JB, Priestley MJN, Park R. Theoretical stress-strain model for confined concrete. J. Struct. Eng. 1998;114(8):1804–26.
[30] PEER Ground Motion Database, NGA-West2. http://ngawest2.berkeley.edu/.
[31] Bulut Fatih. Different phases of the earthquake cycle captured by seismicity along the North Anatolian Fault. Geophys Res Lett 2015;42(7):2219–27.
[32] Silahtar Ali, Budakoğlu Emrah, Horasan Gündüz, Yıldırım Eray, Serdar Küyük H, Yavuz Evrim, et al. Investigation of site properties in Adapazarı, Turkey, using microtremors and surface waves. Environ Earth Sci 2016;75(20). https://doi.org/10.1007/s12665-016-6151-y.
[33] OYO. Production of microzonation report and maps on Anatolian Side. Final Report to Istanbul Metropolitan Municipality.
[34] Panella Dante Sebastian, Tornello Miguel E, Frau Carlos D. A simple and intuitive procedure to identify pulse-like ground motions. Soil Dyn Earthquake Eng 2017;94:234–43.
[35] Güllü A. Determination of the Inelastic Displacement Demand and Response Control of Steel Frame Type Structures by Seismic Energy Equations. PhD Dissertation. Istanbul Technical University; 2018.
[36] Güllü A, Yüksel E. Piece-Wise Exact Computation of Seismic Energy Balance Equation. Italy: Riva del Garda; 2019.
[37] Reyes Juan C, Kalkan Erol. How many records should be used in an ASCE/SEI-7 ground motion scaling procedure? Earthquake Spectra 2012;28(3):1223–42.

[38] Güllü A, Yüksel E, Yalçın C, Dindar AA, Özkaynak H, Büyüköztürk O. An improved input energy spectrum by the shake table tests. Earthquake Eng Struct Dyn 2019;48 (1):27–45.

[39] Yalçın C, Dindar AA, Yüksel E, Özkaynak H, Büyüköztürk O. Seismic design of RC frame structures based on energy-balance method. Eng Struct 2021;237:112220.

[40] Vargas-Alzate YF, Hurtado J. Efficiency of intensity measures considering near- and far-fault ground motion records. Geosciences (Switzerland), 11(6):234.